Süleyman Demirel Üniversitesi Fen Edebiyat Fakültesi Fen Dergisi https://dergipark.org.tr/sdufeffd
Süleyman Demirel University Faculty of Arts and Sciences Journal of Science e-ISSN: 1306-7575
Research Article, 2023, 18(3): 223-237, DOI: 10.29233/sdufeffd.1237412

Influence of Ho Substitution on Structural, Morphological, and Optical Properties of Anatase $Ti_{1-x}Ho_xO_2$ (x= 0.0, 0.01, 0.02, 0.03) Thin Films

Şeydanur Kaya[1,2,*]

[1] Central Research Laboratory, Kastamonu University, 37100, Kastamonu, TURKEY
[2] Department of Physics, Faculty of Sciences, Kastamonu University, 37100, Kastamonu, TURKEY
https://orcid.org/0000-0002-6894-9082
*corresponding author: seydanurkaya@kastamonu.edu.tr

(Received: 17.01.2023, Accepted: 26.09.2023, Published: 23.11.2023)

Abstract: $Ti_{1-x}Ho_xO_2$ (x= 0.0, 0.01, 0.02, 0.03) thin films are synthesized by a sol-gel method and deposited by a dip-coating technique on the glass substrates. The films' crystal structures are examined by an X-ray diffraction technique, while the morphological properties are investigated by scanning electron microscopy and atomic force microscopy. UV-Vis and photoluminescence spectrophotometry are used to analyze the optical properties. Based on the X-ray diffraction patterns, all the films belong to the anatase phase. It is observed that the surface characteristics, such as the morphology, film thickness, and roughness change significantly with the holmium substitution. The optical investigations reveal that the transmittance, band gap energies, and luminescence properties can be adjusted by the holmium substitution. According to the current study, holmium substituted TiO_2 thin films with improved optical properties may be a suitable candidate for applications that require a wide band gap and high optical transparency as well as luminescence properties.

Key words: TiO_2 thin films, Ho substitution, Optical transmittance, Photoluminescence properties

1. Introduction

Titanium dioxide (TiO_2) is one of the most attractive metal oxides with wide band gap (~3.00–4.16 eV) and high optical transmittance [1,2]. TiO_2 is also a promising semiconductor due to its high transparency, refractive index, ultraviolet absorption, and photocatalytic activity, making it suitable for the development of next-generation optoelectronic devices, including photocatalytic systems, optical sensors, photodiodes, phototransistors, solar cells, LEDs, and OLEDs [3]. Furthermore, due to its nontoxicity and biocompatibility, TiO_2 is commonly used in various biotechnological applications such as antibacterial utilities, medicines, air/water purification systems, and cosmetics. Its long-term physical and chemical stability in addition to low-cost and practical synthesis methods are significant advantages for device applications.

Different crystallographic phases, including anatase, rutile, and brookite of TiO_2 can be synthesized by changing the production conditions, such as temperature and pressure. However, rutile and anatase phases are the most commonly used phases in optical applications. Fabrication of TiO_2, in particular, as a thin film rather than as a bulk offers the opportunity for it to be deposited onto different substrates, which enables the production of flexible devices [4]. There are many methods, including chemical spray pyrolysis, electron-beam evaporation, RF sputtering, chemical vapor deposition, and pulsed laser deposition to produce anatase TiO_2 thin films [5–9]. Due to these methods'

complex, expensive, and time-consuming manufacturing processes, researchers have focused on wet chemical methods, such as hydrothermal, chemical bath, and sol-gel, which give desired results in thin film deposition. Among them, the sol-gel method is one of the most attractive methods due to its simple, inexpensive, fast, and practical production processes. This method makes it possible to produce pure and homogeneous thin films with a controllable stoichiometry at relatively lower temperatures. In addition, it enables the fabrication of thin films with different morphologies and optical properties by changing the solution chemistry and the deposition parameters. The sol-gel method with deposition techniques, such as dip-coating and spin-coating provides high-quality thin films with stable optical properties [10]. Thin film surface properties, including grain distribution, size and orientation, film thickness, and roughness play crucial roles in the optical properties of TiO_2. Many previous studies have revealed the strong relationships between the morphological properties and optical properties of TiO_2 thin films [11,12].

Various strategies have been developed to modify the current properties of TiO_2 thin films, such as doping with metal or nonmetal ions, forming oxygen vacancies in the crystal lattice, deposition of various noble metals, combinations with other semiconductors, and interfacial modifications [13]. Undoubtedly, the most practical and effective method among these is doping to the semiconductor's crystal structure. A typical doping process is based on the controlled incorporation of foreign atoms into the crystal lattice. Doping even a small amount of foreign atoms can change the band gap of the semiconductor, increase the amount of charge carriers, and significantly improve the emission properties. In regard to doping studies carried out so far, different factors exist that can affect the final sample, such as production methods and parameters, types of precursor materials and ratios, and solvents. Therefore, each doping processing method should be evaluated within itself in terms of its conditions [14,15]. Namely, even if the same element is doped, different results can be obtained. The doping of rare earth elements (REs) is one of the most effective techniques for the structural and morphological manipulation of TiO_2 as a semiconductor [16]. RE^{3+} ions provide superior electronic, optical, and chemical properties in a wide range of applications due to their 4f electron configuration. Among RE^{3+} ions, holmium (Ho) is one of the most attractive metals due to its large atomic radius and luminescence properties originating from the f-f electronic transition within the partially filled 4f orbitals. By optimizing the doping process of Ho^{3+} ions, it is possible to tune the band gap and optical characteristics of TiO_2 by introducing impurity energy levels into the electronic structure [17]. In addition, the combination of titanium and holmium atoms creates several oxide forms, providing a high magnetic moment, susceptibility, and dielectric permittivity [18]. Compared to other REs, however, fewer studies were conducted on Ho doping on TiO_2. The existing reports mainly focus on its photocatalytic, photovoltaic, magnetic, optoelectronic, and piezoelectric properties [19–23]. However, in these reports, powder or bulk forms of titania, rutile or oxide-mixed crystal phases have been investigated. To our knowledge, no detailed report has been published on the structural and optical properties of Ho doped anatase TiO_2 thin films produced by the sol-gel based dip coating technique. Thus, in this study, the effect of holmium (Ho) on the morphological and optical properties of anatase TiO_2 was investigated. $Ti_{1-x}Ho_xO_2$ (x= 0.0, 0.01, 0.02, 0.03) thin films were produced via a sol-gel method. The influence of Ho substitution on the structural, morphological, and optical properties was examined by various techniques and significant changes were reported.

2. Materials and Methods

A sol-gel method was used to prepare the aqueous solution and a dip-coating technique was used for the deposition of the thin films. A schematic diagram of the preparation of the samples is given in Figure 1. All the films were deposited on a glass substrate using a 0.5 M aqueous solution containing titanium (IV) butoxide ($Ti(OCH_2CH_2CH_2CH_3)_4$) and holmium(III) nitrate pentahydrate ($Ho(NO_3)_3 \cdot 5H_2O$) as precursor materials. A substitutional doping process was carried out. Ethanol was used as a solvent and acetylacetone was used as a chelating agent. A mixture of hydrochloric acid and distilled water was added to the solution dropwise for hydrolysis. The final solution was stirred for two hours at room temperature. After aging overnight, ultrasonically cleaned glass substrates were dip-coated five times. Finally, an annealing process at 600 °C for one hour was applied to all the samples to obtain an anatase crystal phase. An X-ray diffractometer (PANalytical, Empyrean) was used to analyze the crystal structure, while a scanning electron microscope (FEI, Quanta FEG 250) and an atomic force microscope (Bruker, EDGE 3-SYS) were used to examine the surface morphology of the films. A UV-Vis spectrophotometer (Shimadzu, UV Pharmaspec 1700) was used to investigate the optical transmittance, whereas a photoluminescence spectrophotometer (Horiba, FluoroMax-4) equipped with a Xenon lamp was used to analyze the luminescence properties of the samples. The excitation wavelength used was 365 nm.

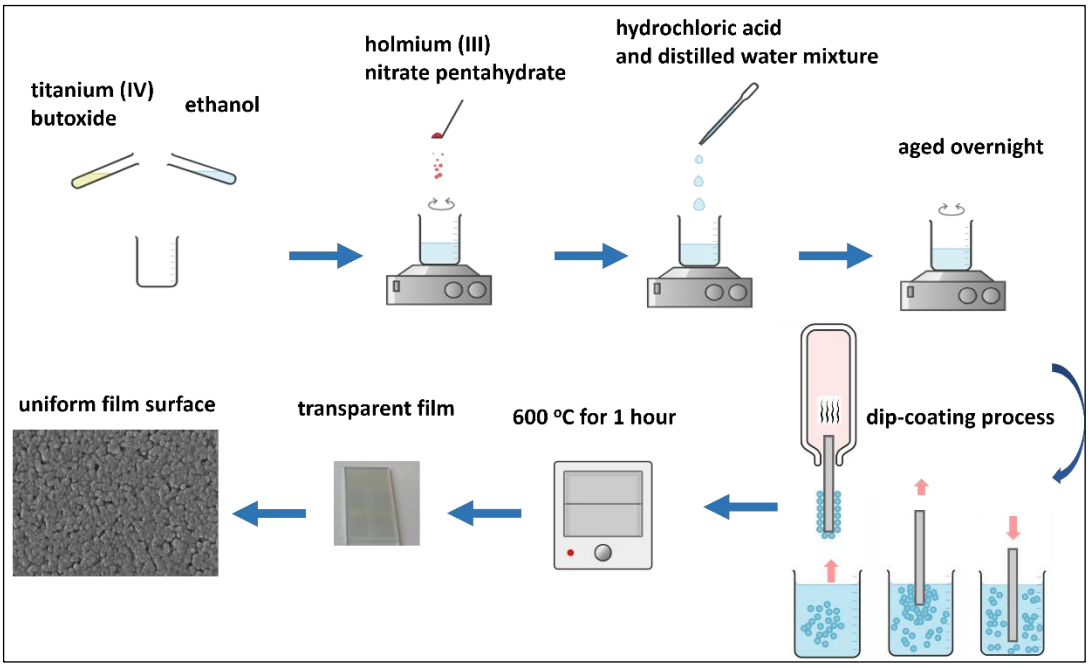

Figure 1. Schematic diagram of the preparation of $Ti_{1-x}Ho_xO_2$ (x= 0.0, 0.01, 0.02, 0.03) thin films

3. Results

The X-ray diffraction patterns of the samples are given in Figure 2. All samples belong to the tetragonal anatase phase of TiO_2 with the diffraction peaks of (101) and (200). There is preferential growth along the (101) surface due to its lowest surface energy [24]. While no impurity peaks are observed in the undoped TiO_2, the impurity peaks of the diholmium titanate (Ho_2TiO_5) phase are detected with increasing Ho concentration. Thus, it can be said that some of the dopant ions do not enter the crystal lattice but instead form the Ho_2TiO_5 based secondary crystal phases, which reach a considerably high intensity level in $Ti_{0.97}Ho_{0.03}O_2$. Furthermore, a slight increase is observed in the intensity of both the (101) and (200) peaks with increasing Ho concentration.

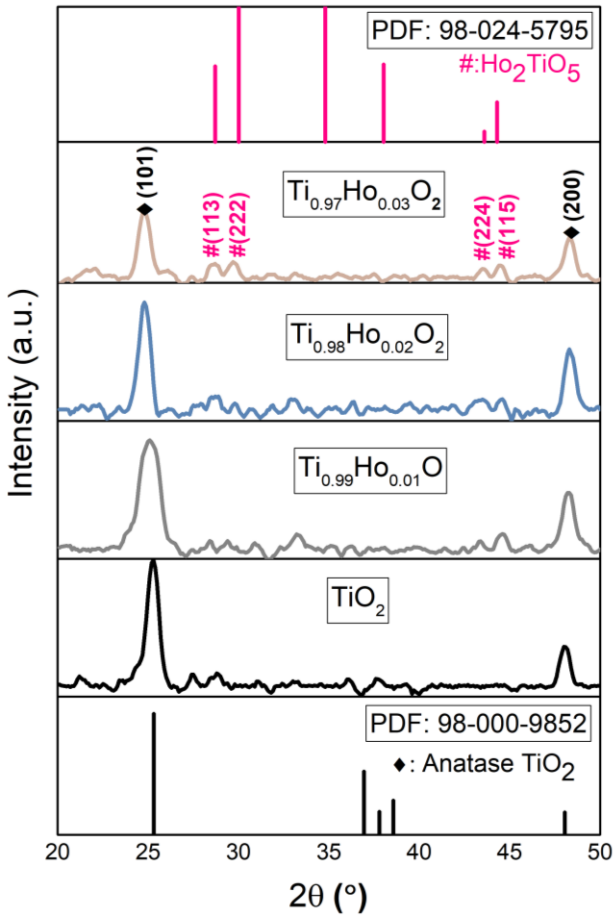

Figure 2. X-ray diffraction patterns of $Ti_{1-x}Ho_xO_2$ (x= 0.0, 0.01, 0.02, 0.03)

The lattice parameters, crystallite size, lattice strain, and dislocation density values of the samples are summarized in Table 1. The lattice parameters for a tetragonal crystal system are calculated by the Bragg's law, which is given below [25]:

$$\frac{1}{d^2} = \frac{h^2 + k^2}{a^2} + \frac{l^2}{c^2} \tag{1}$$

where, d is the interplanar spacing between the crystal planes, h, k, l are the Miller indices, a and c ($a = b \neq c$) are the lattice parameters of the tetragonal crystal system. The crystallite size values of the samples are determined using the Scherrer equation, which is given as [25]:

$$D = 0.941\lambda/\beta cos\theta \tag{2}$$

where D is the crystallite size, λ is the wavelength of the X-ray, β is the full width at half maximum (FWHM), and θ is the diffraction angle. The microstrain values are calculated using the formula given below [26]:

$$\varepsilon = \frac{\beta cos\theta}{4sin\theta} \tag{3}$$

Finally, for the density dislocation calculations, the Williamson–Hall relation is used as given below [27]:

$$\delta = \frac{1}{D^2} \tag{4}$$

where β is the (FWHM), θ is the diffraction angle, and D is the crystallite size.

Table 1. Lattice parameters, crystallite size, lattice strain, dislocation density, and film thickness values of $Ti_{1-x}Ho_xO_2$ (x= 0.0, 0.01, 0.02, 0.03)

Sample	Lattice parameters a (Å)= b (Å)	c (Å)	Crystallite size (nm)	Microstrain (10^{-3})	Discolation Density (10^{-3}) (nm^{-2})	Film thickness (nm)
TiO_2	3.78	9.49	13	12.63	5.91	60.93
$Ti_{0.99}Ho_{0.01}O_2$	3.93	9.21	9	19.01	12.3	68.14
$Ti_{0.98}Ho_{0.02}O_2$	3.80	9.65	11	14.25	8.26	75.02
$Ti_{0.97}Ho_{0.03}O_2$	3.66	9.29	12	13.69	6.94	82.34

According to Table 1, the a lattice parameter of undoped TiO_2 is 3.78 Å, while it increases to 3.93 Å for $Ti_{0.99}Ho_{0.01}O_2$. Then, a gradual decrease is observed in the a lattice parameter values with increasing Ho substitution ratio and reaches its minimum in $Ti_{0.97}Ho_{0.03}O_2$. The Ho^{3+} ions have a larger ionic radius (0.901 Å) than that of the Ti^{4+} ions (0.605 Å). Thus, the incorporation of Ho^{3+} ions into the Ti^{4+} sites is expected to create lattice expansion and tensile microstrain in the TiO_2 [28]. At 1% Ho, the increment of the a lattice parameter indicates that the Ho^{3+} ions cause an expansion along the a-direction of the TiO_2 tetragonal lattice. This result is in agreement with the highest tensile microstrain value of $Ti_{0.99}Ho_{0.01}O_2$ given in Table 1. It is also interesting to note that the Ho_2TiO_5 phase begins to form in this sample, which is shown by weak XRD peaks yet do not affect the substitution process, according to the crystal parameters (Table 1). As the Ho concentration increases, the substitution ratio decreases, and unsubstituted Ho^{3+} ions promote further formation of the Ho_2TiO_5 phase. Accordingly, the expansion along the a-direction tends to decrease at relatively higher Ho concentrations. Previously, the increment up to a certain doping level and then decrement of the a lattice parameter has been observed in ZnO thin films and has been associated with the difference in dopant ionic radii, which is also supported by our current results [29]. The c lattice parameter is 9.49 Å for the undoped sample and decreases to 9.21 Å for $Ti_{0.99}Ho_{0.01}O_2$. While a slight increase is observed in $Ti_{0.98}Ho_{0.02}O_2$, it decreases in $Ti_{0.97}Ho_{0.03}O_2$. These variations in lattice parameters can be attributed to the different incorporation rates of Ho^{3+} ions into the TiO_2 host crystal lattice as well as the formation of the Ho_2TiO_5 phase. The crystallite size values are 13 nm, 9 nm, 11 nm, and 12 nm for TiO_2, $Ti_{0.99}Ho_{0.01}O_2$, $Ti_{0.98}Ho_{0.02}O_2$, and $Ti_{0.97}Ho_{0.03}O_2$, respectively. Positive microstrain values are observed for all the samples, confirming the tensile strain of the lattice (Table 1). The undoped sample has the lowest microstrain value. At 1% Ho, a significant increase occurs in the microstrain of $Ti_{0.99}Ho_{0.01}O_2$, and then, with increasing Ho concentration, shows a gradual decrease to a value still higher than the undoped one. This observation aligns with a similar result reported previously, which confirms that Ho ions result in a distortion in the TiO_2 crystal lattice [19]. This enhancement in the microstrain might be caused by several factors, such as crystal defects, lattice mismatch, and the difference between the ionic radius of the dopants and the host ions [30,31]. Dislocations can be defined as imperfections in a crystal, while dislocation density describes the dislocation lines per unit volume of the crystals [32]. According to the dislocation density values given in Table 1, the incorporation of Ho^{3+} ions into the TiO_2 lattice creates lattice distortions, which is attributed to the defect concentration.

Figure 3 shows the top and cross-sectional SEM images of the $Ti_{1-x}Ho_xO_2$ (x= 0.0, 0.01, 0.02, 0.03) thin films. As shown in Figure 3(a), undoped TiO_2 has a homogenous surface distribution of uniformly sized spherical particles. With the incorporation of Ho^{3+} ions into the crystal structure, at a concentration of 1%, the surface morphology significantly changes. Many more grain formations with different shapes including both smaller and larger particles are observed, compared with that of the undoped sample (Figure 3(b)). When the Ho concentration is 2%, the number of large particles decreases (Figure 3(c)). At 3% Ho, quite large polyhedral clusters with sharp edges are observed on the surface

(Figure 3(d)). Thus, it can be said that the surface is quite far from a uniform distribution at 3% Ho.

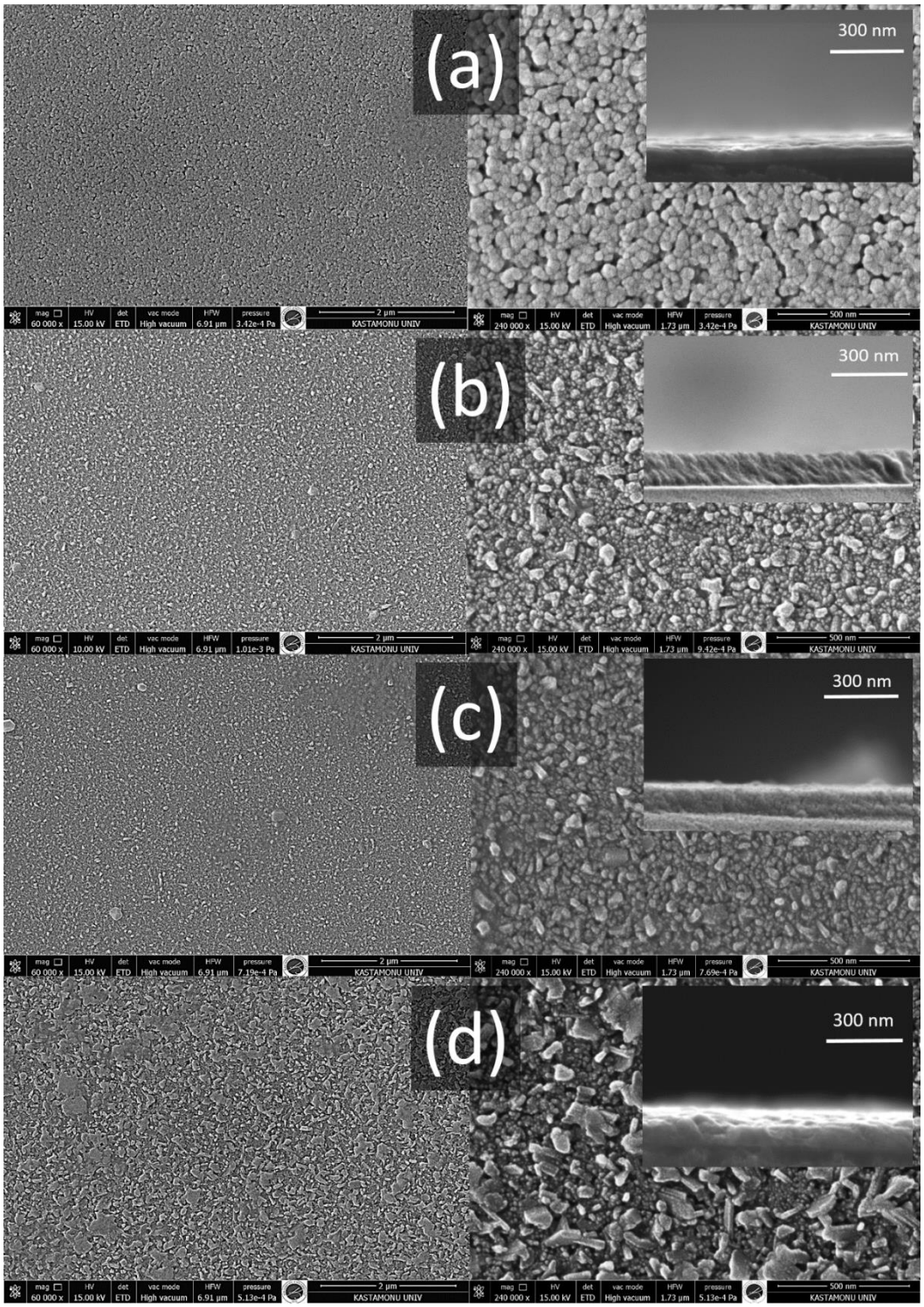

Figure 3. Top and cross-sectional (shown in inset) SEM views of (a) TiO_2, (b) $Ti_{0.99}Ho_{0.01}O_2$, (c) $Ti_{0.98}Ho_{0.02}O_2$, and (d) $Ti_{0.97}Ho_{0.03}O_2$

The film thicknesses were measured from the cross-sectional SEM views of the films and are given in Table 1. The film thicknesses are 60.93 nm, 68.14 nm, 75.02 nm, and 82.34 nm for TiO_2, $Ti_{0.99}Ho_{0.01}O_2$, $Ti_{0.98}Ho_{0.02}O_2$, and $Ti_{0.97}Ho_{0.03}O_2$, respectively. It can be concluded that the thickness of the films increases gradually with Ho substitution. EDX area analysis spectra of the samples are given in Figure 4, while the mapping results of $Ti_{0.97}Ho_{0.03}O_2$ is given in Figure 5. The elemental concentrations of all the samples are given in Table 2. In addition to Ti, O, and Ho peaks, the spectra include some impurity peaks such as Si and Na, which come from the substrate used, as well as, Au peaks, which

come from the conductive coating of SEM measurements. For the undoped sample, the elemental concentrations of Ti and O are 33.32 and 66.68 (atomic %), respectively. For $Ti_{0.97}Ho_{0.03}O_2$, the elemental concentrations of Ti, O, and Ho are 29.28, 65.87, and 4.85 (atomic %), respectively. The mapping images confirm the homogeneous distribution of the Ho^{3+} ions in the TiO_2 microstructure.

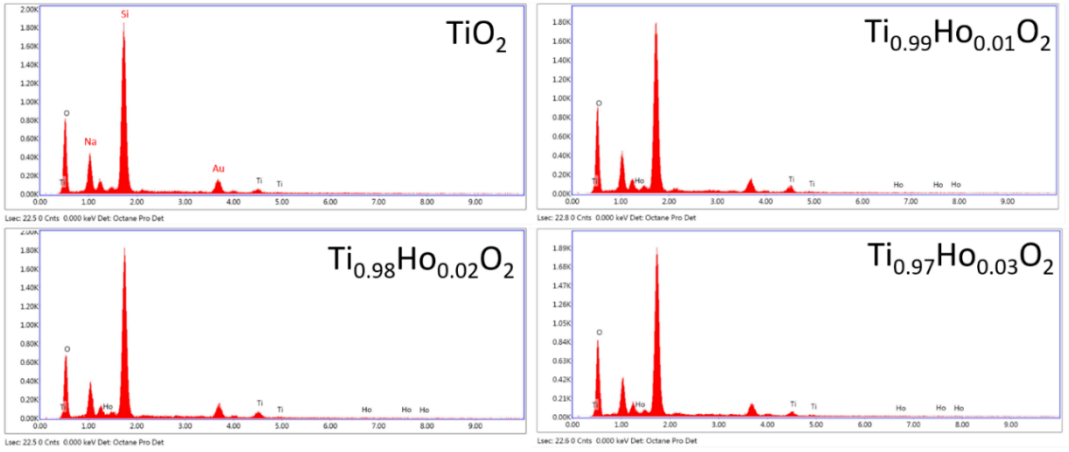

Figure 4. EDX analysis spectra of $Ti_{1-x}Ho_xO_2$ (x= 0.0, 0.01, 0.02, 0.03)

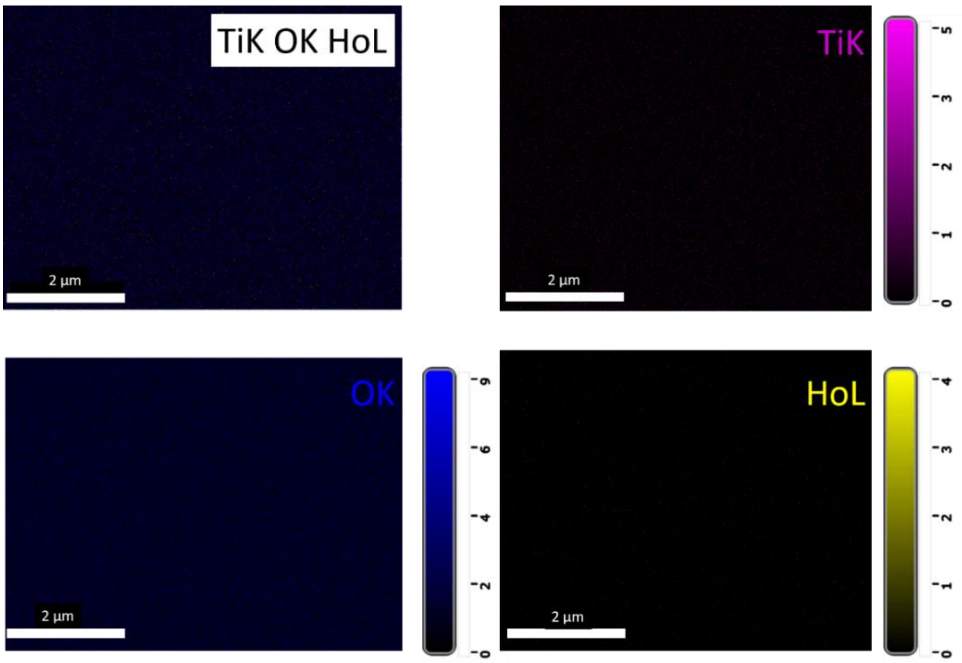

Figure 5. EDX mapping images of $Ti_{0.97}Ho_{0.03}O_2$

Table 2. Elemental concentrations of $Ti_{1-x}Ho_xO_2$ (x= 0.0, 0.01, 0.02, 0.03)

Sample	Element	Atomic (%)
TiO_2	Ti	33.32
	O	66.68
$Ti_{0.99}Ho_{0.01}O_2$	Ti	31.94
	O	65.33
	Ho	2.73
$Ti_{0.98}Ho_{0.02}O_2$	Ti	30.60
	O	66.13
	Ho	3.27
$Ti_{0.97}Ho_{0.03}O_2$	Ti	29.28
	O	65.87
	Ho	4.85

Figure 6 shows the top and perspective AFM views of the $Ti_{1-x}Ho_xO_2$ (x= 0.0, 0.01, 0.02, 0.03) thin films. In all the images, an area of 5x5 μm was scanned. The top views of the film surfaces are shown on the left, while perspective views are shown on the right. According to the images, whereas there is a homogeneous particle distribution in the undoped TiO_2, the clusters forming on the surfaces can clearly be seen in the doped samples, in accordance with the SEM results.

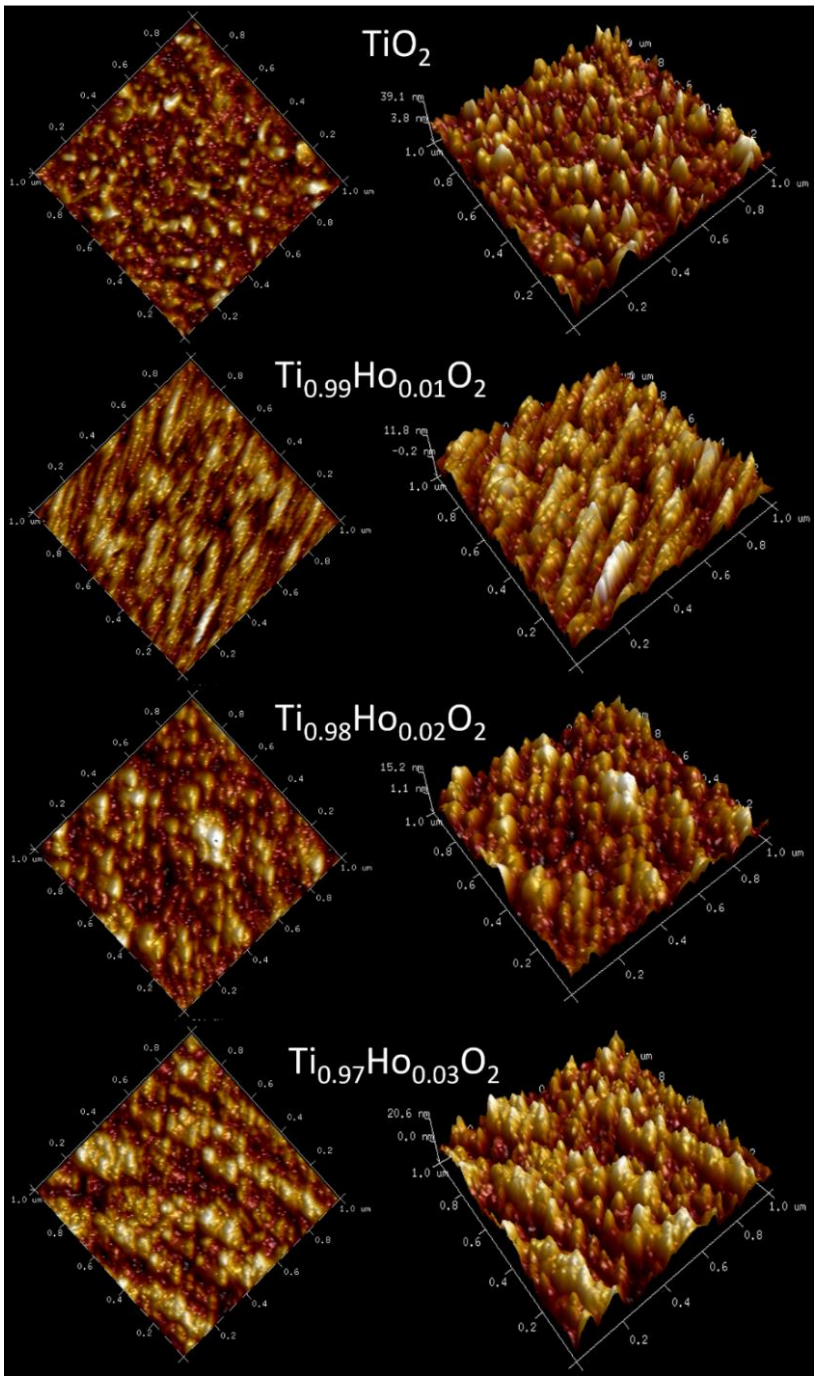

Figure 6. Top (left) and perspective (right) AFM views of $Ti_{1-x}Ho_xO_2$ (x= 0.00, 0.01, 0.02, 0.03)

For a further investigation of the films' surface profile, roughness analyzes were carried out. The roughness parameters of all the samples, including average roughness (R_a), root mean square roughness (R_q), maximum roughness (R_{max}), skewness (R_{sk}), and kurtosis (R_{ku}) are presented in Table 3. The (R_a) is 3.20 nm for undoped TiO_2, which increases to 3.61 nm in $Ti_{0.99}Ho_{0.01}O_2$. When the Ho concentration reaches 2%, the R_a value is obtained as 4.54 nm. Finally, at a concentration of 3% Ho, it reaches its maximum, with

a value of 5.02 nm. The formation of larger particles due to Ho substitution could be responsible for this slight increase in the roughness values due to the variation in height differences on the film surfaces. The R_q value is a measure of the standard deviation of the Z height and is also known as RMS. This parameter defines the roughness by statistical methods, unlike the arithmetic average height (R_a) and gives more precise results than R_a in terms of significant deviation from the reference line [33]. Although R_a is used more frequently in surface roughness definitions, R_q values should also be considered when examining roughness properties. R_q values are obtained as 4.16 nm, 4.58 nm, 6.00 nm, and 6.27 nm for TiO_2, $Ti_{0.99}Ho_{0.01}O_2$, $Ti_{0.98}Ho_{0.02}O_2$, and $Ti_{0.97}Ho_{0.03}O_2$, respectively, showing a gradual increment with Ho substitution. As expected, the R_q values are higher than those of R_a and have the same increasing tendency with Ho concentration rate. Morphological changes previously observed in SEM, such as increasing film thickness, change in grain sizes, formation of clusters on the surface, and formation of secondary oxide phases with Ho substitution, can be attributed to the increase in both R_q and R_a values. The R_{sk} values, which show the degree of asymmetry of the profile about the reference line, are obtained as 0.97, 0.44, 0.88, and 0.24 for TiO_2, $Ti_{0.99}Ho_{0.01}O_2$, $Ti_{0.98}Ho_{0.02}O_2$, and $Ti_{0.97}Ho_{0.03}O_2$, respectively. These positive skewness values mean the peaks are predominantly distributed on all the film surfaces. The R_{ku} values of the samples are obtained as 4.91, 3.67, 4.78, and 3.13 for TiO_2, $Ti_{0.99}Ho_{0.01}O_2$, $Ti_{0.98}Ho_{0.02}O_2$, and $Ti_{0.97}Ho_{0.03}O_2$, respectively. R_{ku} values higher than 3 mean the film surfaces is defined as leptokurtic [33].

Table 3. Roughness parameters of $Ti_{1-x}Ho_xO_2$ (x= 0.00, 0.01, 0.02, 0.03)

Parameters / Samples	R_a (nm)	R_q (nm)	$R_{max}(nm)$	R_{sk}	R_{ku}
TiO_2	3.20	4.16	41.9	0.97	4.91
$Ti_{0.99}Ho_{0.01}O_2$	3.61	5.58	42.6	0.44	3.67
$Ti_{0.98}Ho_{0.02}O_2$	4.54	6.00	51.4	0.88	4.78
$Ti_{0.97}Ho_{0.03}O_2$	5.02	6.27	48.2	0.24	3.13

Figure 7 illustrates the optical transmittance graphs, while Table 4 presents the corresponding average transmittance values of $Ti_{1-x}Ho_xO_2$ (x= 0.0, 0.01, 0.02, 0.03) thin films. The average optical transmittance of the undoped sample in the visible region is 62%. With the Ho substitution, the average optical transmittance is obtained as 65% in $Ti_{0.99}Ho_{0.01}O_2$, while it is 77% in $Ti_{0.98}Ho_{0.02}O_2$, showing a considerable increment. Finally, $Ti_{0.97}Ho_{0.03}O_2$ shows the highest optical transmittance value of 80%. It is clear that Ho substitution improves the optical transmittance of TiO_2 thin films produced by the current method. The increment in the optical transmittance values of TiO_2 thin films by various doping processes has been observed in previous studies [11,16,34]. Many factors, such as film thickness, surface properties, roughness, crystal defects, annealing temperature and conditions, affect film transparency [35,36]. For the current study, the reduction in crystallite size with Ho substitution might hinder the light scattering, causing an increased optical transmittance in the visible region [35,37]. Furthermore, previous studies have emphasized that the transmittance properties are associated with crystal lattice defects [6,36,38]. In particular, the boost observed in the optical transmittance of $Ti_{0.98}Ho_{0.02}O_2$ might be attributed to the sharp decrease in the dislocation density of this sample (Table 1). Moreover, the formation of Ho_2TiO_5 particles might be responsible for the increased light transmission, which also needs further research.

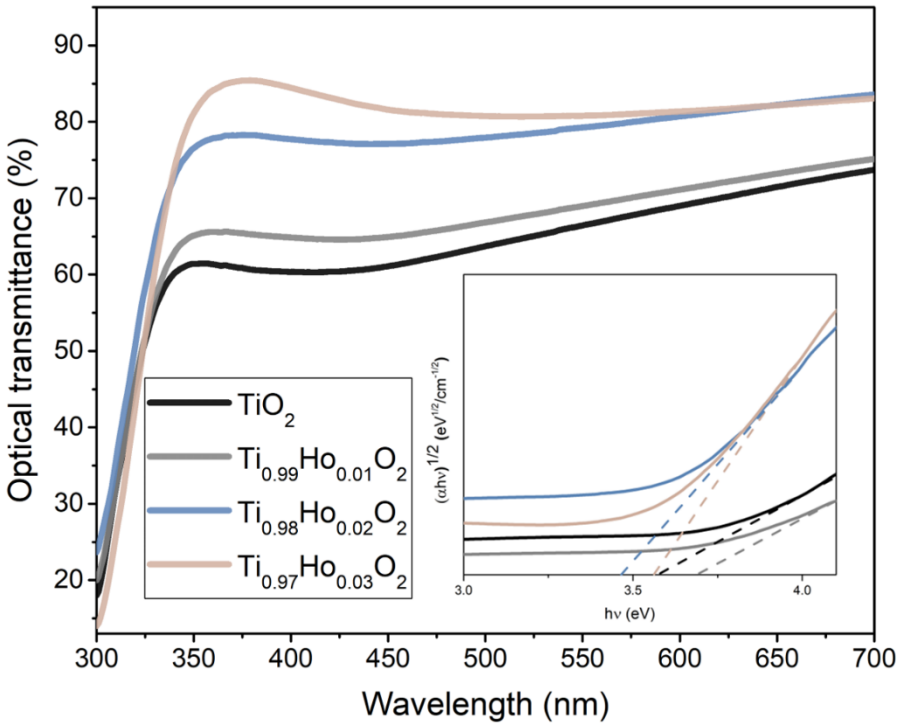

Figure 7. Optical transmittance graphs and Tauc's plots (shown in the inset) of $Ti_{1-x}Ho_xO_2$ (x= 0.0, 0.01, 0.02, 0.03)

Table 4. Average optical transmittance, band gap energy, and refractive index values of $Ti_{1-x}Ho_xO_2$ (x= 0.00, 0.01, 0.02, 0.03)

Sample	Average optical transmittance (%)	Band gap energy (eV)	Refractive index
TiO_2	62	3.58	2.17
$Ti_{0.99}Ho_{0.01}O_2$	65	3.69	2.14
$Ti_{0.98}Ho_{0.02}O_2$	77	3.46	2.20
$Ti_{0.97}Ho_{0.03}O_2$	80	3.56	2.17

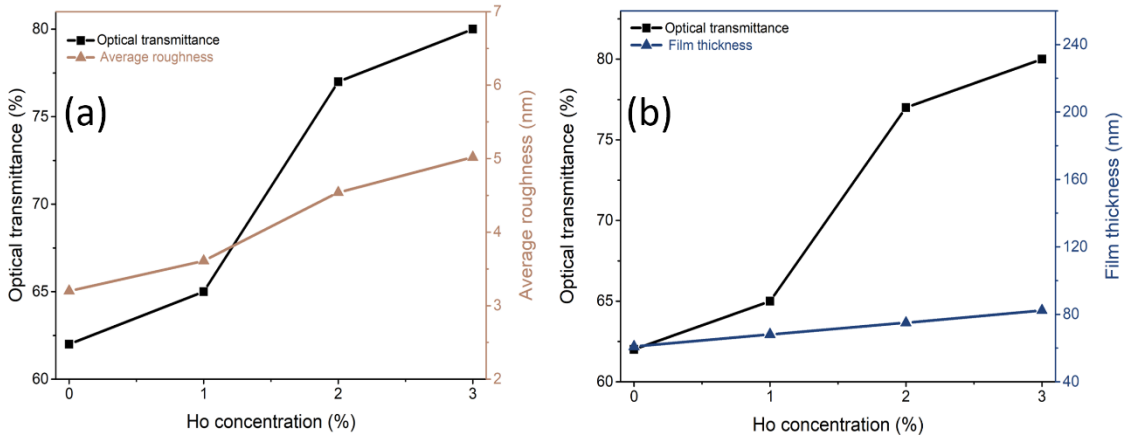

Figure 8. (a) The relationship between the average roughness and the average optical transmittance versus different Ho concentrations, (b) The relationship between the optical transmittance and the film thickness of the films versus different Ho concentrations

Figure 8(a) shows the relationship between the average roughness and the average optical transmittance values of all the samples. According to the graph, films' optical transmittance and roughness values increases with Ho substitution. Accordingly, it can be concluded that roughness-induced light scattering do not suppress an increase in the optical transmittance of the films with Ho substitution [34]. Figure 8(b) shows the

relationship between the optical transmittance values and the film thickness of the samples versus different Ho concentrations. It is clear from the graph that the optical transmittance of the samples increases with the Ho concentration despite an increase in film thickness.

From the transmittance spectrum, the absorption coefficient (α) can be calculated by the equation given below [39]:

$$\alpha = \frac{1}{d}(ln\frac{1}{T}) \quad (5)$$

where T is the transmittance, and d is the thickness of the film. The band gap energy is determined using the equation given as [40]:

$$\alpha = \frac{A(hv - E_g)^n}{hv} \quad (6)$$

where hv is the photon energy, and A is the photon energy independent constant. The exponent n has a value of 1/2 for direct transitions and a value of 2 for indirect transitions. For indirect transitions, the equation can be written as [12]:

$$(\alpha hv)^{1/2} = A\left(hv - E_g\right) \quad (7)$$

The indirect band gap energies (E_g) of the samples were calculated from Tauc's plots, which are given in the inset of Figure 7, showing extrapolation of the linear portion of the plot $(\alpha hv)^{1/2}$ as a function of hv. The E_g values of all the samples are given in Table 4. The values obtained are in agreement with previous reports [6,37]. The E_g values of the samples are calculated as 3.58 eV, 3.69 eV, 3.46 eV, and 3.56 eV for TiO_2, $Ti_{0.99}Ho_{0.01}O_2$, $Ti_{0.98}Ho_{0.02}O_2$, and $Ti_{0.97}Ho_{0.03}O_2$, respectively. The band gap values of TiO_2 thin films are highly dependent on the production methods, electronic structure, chemical compositions and ratios, heat treatment procedures, surface morphology, and crystal properties. A widening in the E_g of $Ti_{0.99}Ho_{0.01}O_2$ can be attributed to the sharp decrease in the crystallite size of this sample (Table 1). On the other hand, a narrowing of E_g in $Ti_{0.98}Ho_{0.02}O_2$ is attributed to the introduction of new impurity levels through substitution [34]. As the Ho concentration increases, factors such as the increase in the crystallite size and the creation of lattice defects might be responsible for the further increase in the E_g of $Ti_{0.97}Ho_{0.03}O_2$ [6].

The refractive indices of the samples were estimated by a general relation between the refractive index and energy gap in semiconductors proposed by Hervé and Vandamme [41]:

$$n^2 = 1 + (\frac{A}{E_g + B})^2 \quad (8)$$

where, A is the hydrogen ionization energy, which equals 13.6 eV, while B is the constant assumed to be the difference between the UV resonance energy and band gap energy, and equals 3.47 eV [29,42]. Refractive index (n) values are given in Table 4. The n value is obtained as 2.17 for the undoped sample, while it is 2.14 for $Ti_{0.99}Ho_{0.01}O_2$. After showing the maximum value of 2.20 for $Ti_{0.98}Ho_{0.02}O_2$, interestingly, it decreases again to 2.17 in $Ti_{0.97}Ho_{0.03}O_2$. In previous studies, an increment [16,43], a decrement [44], and fluctuations [45] of the refractive index of TiO_2 with doping have been observed. The change in the refractive index has been associated with different factors such as crystal phase, crystallite size, annealing temperature, packing density, porosity, and film density

[46]. In addition, condensation and evaporation processes during the preparation of sol-gel based materials as well as the heat treatment and withdrawal speed of the substrate during the dip coating processes may also be responsible for the changes in the reactive index by affecting the surface characteristics [47].

The photoluminescence (PL) emission spectra of $Ti_{1-x}Ho_xO_2$ (x= 0.0, 0.01, 0.02, 0.03) thin films are given in Figure 9. All the samples exhibit a broad visible emission band ranging from 460 to 600 nm. The undoped sample's emission band is centered at 526 nm, while a slight blueshift is observed at 1% and 2% Ho. The peak center of the emission band is measured as 524 and 523 nm for $Ti_{0.99}Ho_{0.01}O_2$ and $Ti_{0.98}Ho_{0.02}O_2$, respectively. At 3% Ho, the peak center is 524 nm for $Ti_{0.97}Ho_{0.03}O_2$. The emission intensity of the samples increases as the Ho concentration is raised to 2%. The maximum emission is observed in $Ti_{0.98}Ho_{0.02}O_2$, and then it shows a sharp reduction in $Ti_{0.97}Ho_{0.03}O_2$. In the case of doped TiO_2 thin films, it has been previously observed that PL emissions are quenched or even disappear at higher doping ratios [48,49]. The variation in PL intensity is attributed to the change in defect states on the shallow level of the thin film surfaces [50]. Thus, it can be inferred that the recombination rate of photogenerated electrons and holes on the shallow level of the film sharply decreases in $Ti_{0.97}Ho_{0.03}O_2$ [50,51]. In addition to these results, it is noteworthy that the intense formation of the Ho_2TiO_5 as a secondary phase could be also responsible for the PL quenching in $Ti_{0.97}Ho_{0.03}O_2$.

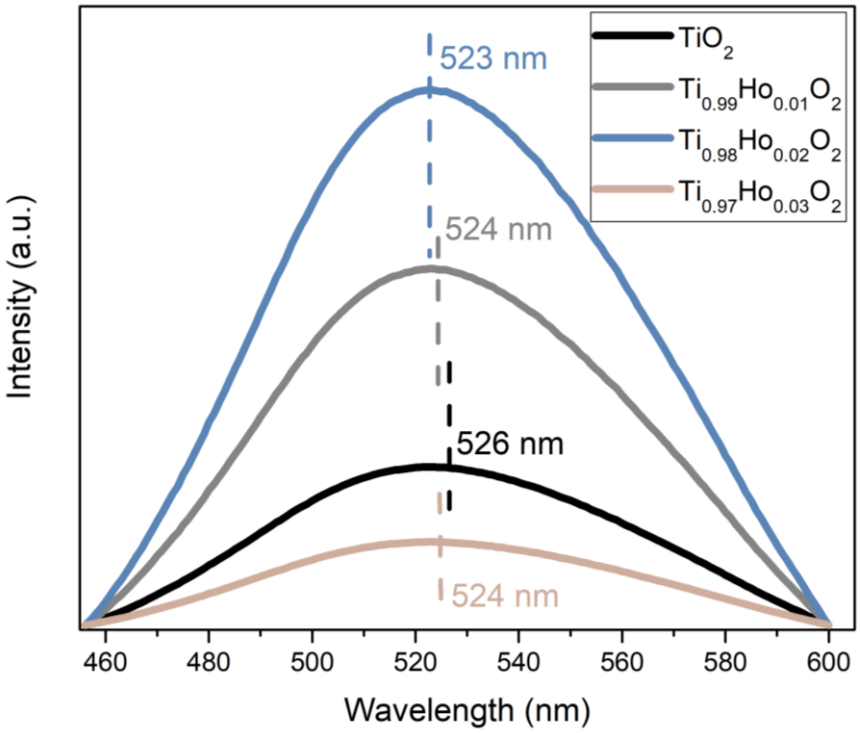

Figure 9. PL emissions of $Ti_{1-x}Ho_xO_2$ (x= 0.0, 0.01, 0.02, 0.03)

4. Conclusion

$Ti_{1-x}Ho_xO_2$ (x= 0.0, 0.01, 0.02, 0.03) thin films were prepared by a sol-gel method and a dip-coating technique. The influence of Ho substitution on the crystallographic, morphologic, and optical properties of TiO_2 thin films was investigated. According to the X-ray diffraction analyzes, all the films belong to the anatase phase of TiO_2. Nevertheless, with increasing Ho concentration, a secondary phase of Ho_2TiO_5 is observed. SEM images show that Ho substitution has significant effects on the morphological properties of TiO_2 thin films. The AFM measurements reveal that the Ho substitution increases the average roughness of the TiO_2 thin films. The increase in both the thickness and

roughness values of the films with the increase in Ho concentration does not hinder the enhancement of the optical transmittance of the samples. Furthermore, the visible region PL emission increases as the Ho concentration is increased up to 2%, and then decreases sharply at 3% Ho, indicating that a quenching occurs in substituted samples beyond a certain level (2% for the current study). Overall, it can be concluded that Ho substitution at relatively lower rates (x < 3%) is an efficient way to improve the optical properties of TiO_2 thin films, which are good candidates for next-generation optoelectronic applications.

Authorship contribution statement

Ş. Kaya: Conceptualization, Methodology, Investigation, Original Draft Writing, Review and Editing.

Declaration of competing interest

The authors declare that they have no known competing financial interests or personal relationships that could have appeared to influence the work reported in this paper.

Acknowledgment

This study was funded by the Kastamonu University Scientific Research Projects Coordination Department under Grant No. [KU-BAP01/2021-05].

Ethics Committee Approval and/or Informed Consent Information

As the authors of this study, we declare that we do not have any ethics committee approval and/or informed consent statement.

References

[1] A. M. E. Raj, V. Agnes, V. Bena Jothy, C. Ravidhas, J. Wollschläger, M. Suendorf, M. Neumann, M. Jayachandran and C. Sanjeeviraja, "Spray deposition and property analysis of anatase phase titania (TiO 2) nanostructures", *Thin Solid Films*, 519, 129-135,2010.

[2] T. C. Paul, M. H. Babu, J. Podder, B. C. Dev, S. K. Sen and S. Islam, "Influence of Fe3+ ions doping on TiO2 thin films: Defect generation, d-d transition and band gap tuning for optoelectronic device applications", *Physica B: Condensed Matter*, 604, 412618,2021.

[3] T. S. Rajaraman, S. P. Parikh and V. G. Gandhi, "Black TiO2: A review of its properties and conflicting trends", *Chemical Engineering Journal*, 389, 123918,2020.

[4] A. Farzaneh, M. Javidani, M.D. Esrafili and O. Mermer, "Optical and photocatalytic characteristics of Al and Cu doped TiO2: Experimental assessments and DFT calculations", *Journal of Physics and Chemistry of Solids*, 161, 110404, 2022.

[5] A. Möllmann, D. Gedamu, P. Vivo, R. Frohnhoven, D. Stadler, T. Fischer, I. Ka, M. Steinhorst, R. Nechache, F. Rosei, S.G. Cloutier, T. Kirchartz and S. Mathur, "Highly Compact TiO 2 Films by Spray Pyrolysis and Application in Perovskite Solar Cells", *Advance Engineering Materials*, 4,1801196, 2019.

[6] C. Yang, H. Fan, Y. Xi, J. Chen and Z. Li, "Effects of depositing temperatures on structure and optical properties of TiO 2 film deposited by ion beam assisted electron beam evaporation", *Applied Surface Science*, 44 (15), 2996-3000, 2008.

[7] D. Mardare, M. Tasca, M. Delibas and G. I. Rusu, "On the structural properties and optical transmittance of TiO2 r.f. sputtered thin films", *Applied Surface Science*, 156 (1-4), 200-206, 2000.

[8] D.S. Bhachu, R.G. Egdell, G. Sankar, C.J. Carmalt and I.P. Parkin, "Electronic properties of antimony-doped anatase TiO2 thin films prepared by aerosol assisted chemical vapour deposition", *Journal of Materials Chemistry C*, 5 (37), 9694-9701, 2017.

[9] J .C. Orlianges, A. Crunteanu, A. Pothier, T. Merle-Mejean, P. Blondy and C. Champeaux, "Titanium dioxide thin films deposited by pulsed laser deposition and integration in radio frequency devices: Study of structure, optical and dielectric properties", *Applied Surface Science*, 263, 111-114,2012.

[10] S. Obregón and V. Rodríguez-González, "Photocatalytic TiO2 thin films and coatings prepared by

sol–gel processing: a brief review", *Journal of Sol-Gel Science and Technology*, 102,125-141, 2021.

[11] Z. Lu, X. Jiang, B. Zhou, X. Wu and L. Lu, "Study of effect annealing temperature on the structure, morphology and photocatalytic activity of Si doped TiO 2 thin films deposited by electron beam evaporation", *Applied Surface Science*, 257 (24), 10715-10720, 2011.

[12] S. K. Gupta, J. Singh, K. Anbalagan, P. Kothari, R. R. Bhatia, P. K. Mishra, V. Manjuladevi, R. K. Gupta and J. Akhtar, "Synthesis, phase to phase deposition and characterization of rutile nanocrystalline titanium dioxide (TiO 2) thin films", *Applied Surface Science*, 264, 737-742, 2013.

[13] Y. Lv, H. Tong, W. Cai, Z. Zhang, H. Chen, X. Zhou, "Boosting the efficiency of commercial available carbon-based perovskite solar cells using Zinc-doped TiO2 nanorod arrays as electron transport layer", *Journal of Alloys and Compounds*, 851, 156785, 2021.

[14] H. N. T. Phung, N. D. Truong, L. T. Nguyen, K. L. P. Thi, P. A. Duong and V.T.H. Le, "Enhancement of the visible light photocatalytic activity of vanadium and nitrogen co-doped TiO2 thin film", *Journal of Nonlinear Optical Physics & Materials*, 24 (4), 1550052, 2015.

[15] M. H. Chan, W. Y. Ho, D. Y. Wang and F. H. Lu, "Characterization of Cr-doped TiO2 thin films prepared by cathodic arc plasma deposition", *Surface Coatings Technology*, 202 (4-7), 962–966, 2007.

[16] D. Komaraiah, E. Radha, J. Sivakumar, M. V. Ramana Reddy and R. Sayanna, "Photoluminescence and photocatalytic activity of spin coated Ag+ doped anatase TiO2 thin films", *Optical Materials*, 108, 110401, 2020.

[17] B. Singaram, J. Jeyaram, R. Rajendran, P. Arumugam and K. Varadharajan, "Visible light photocatalytic activity of tungsten and fluorine codoped TiO2 nanoparticle for an efficient dye degradation", *Ionics*, 25 (2), 773–784, 2019.

[18] K. Kukli, M. Kemell, M. C. Dimri, E. Puukilainen, A. Tamm, R. Stern, M. Ritala and M. Leskelä, "Holmium titanium oxide thin films grown by atomic layer deposition", *Thin Solid Films*, 565, 261–266, 2014.

[19] J. wen Shi, J. tang Zheng and P. Wu, "Preparation, characterization and photocatalytic activities of holmium-doped titanium dioxide nanoparticles", *Journal of Hazardous Materials*, 161(1), 416–422, 2009.

[20] J. Shi, J. Zheng, Y. Hu and Y. Zhao, "Photocatalytic degradation of organic compounds in aqueous systems by Fe and Ho codoped TiO2", *Kinetics and Catalysis*, 49, 279–284, 2008.

[21] F. Peng and D. Zhu, "Effect of sintering temperature and Ho2O3 on the properties of TiO2-based varistors", *Ceramics International*, 44, 21034–21039, 2018.

[22] T. M. Pan, M. De Huang, C. W. Lin and M. H. Wu, "Development of high-κ HoTiO3 sensing membrane for pH detection and glucose biosensing", *Sensors & Actuators, B: Chemical*, 144, 139–145, 2010.

[23] L. Macalik, M. Maczka, P. Solarz, A. F. Fuentes, K. Matsuhira and Z. Hiroi, "Optical spectroscopy of the geometrically frustrated pyrochlore Ho2Ti2O7", *Optical Materials*, 31, 6, 790–794, 2009.

[24] G. Li, K. Fang, Y. Ou, W. Yuan, H. Yang, Z. Zhang and Y. Wang, "Surface study of the reconstructed anatase TiO2 (001) surface", *Progress in Natural Science*, 31,1, 2021.

[25] D. Komaraiah, E. Radha, N. Kalarikkal, J. Sivakumar, M. V. Ramana Reddy and R. Sayanna, "Structural, optical and photoluminescence studies of sol-gel synthesized pure and iron doped TiO2 photocatalysts", *Ceramics International*, 45, 25060–25068, 2019.

[26] Y. Doubi, B. Hartiti, L. Hicham, S. Fadili, A. Batan, M. Tahri, A. Belfhaili and P. Thevnin, "Effect of annealing time on structural and optical proprieties of TiO2 thin films elaborated by spray pyrolysis technique for future gas sensor application", *Materials Today: Proceedings*, 3 (4), 823–827, 2020.

[27] A. M. Bolbol, O. H. Abd-Elkader, H. Elshimy, Z. I. Zaki, S. A. Shata, M. Kamel, A. S. Radwan and N.Y. Mostafa, "The effect of Zr (IV) doping on TiO2 thin film structure and optical characteristics", *Results in Physics*, 42, 2022.

[28] D. Nath, F. Singh and R. Das, "X-ray diffraction analysis by Williamson-Hall, Halder-Wagner and size-strain plot methods of CdSe nanoparticles- a comparative study", *Materials Chemistry and Physics*, 239 (1), 2020.

[29] G. Demircan, E. F. Gurses, B. Aktas, S. Yalcin, A. Acikgoz, G. Ceyhan and M. V. Balak, "Sol–gel synthesis of Si-ZnO, Ti-ZnO and Si-Ti-ZnO thin films: Impact of Si and Ti content on structural and optical properties", *Materials Today Communications*, 34, 105234, 2023.

[30] A. K. Deb and P. Chatterjee, "Microstrain and lattice disorder in nanocrystalline titanium dioxide prepared by chemical route and its relation with phase transformation", *Journal of Theoretical and Applied Physics*,14, 285–293, 2020.

[31] D. Sudha, S. Dhanapandian, C. Manoharan, A. Arunachalam, "Structural, morphological and electrical properties of pulsed electrodeposited CdIn2Se4 thin films", *Results in Physics*, 6, 599–605, 2016.

[32] S. M. AL-Shomar, "Synthesis and characterization of Eu3+ doped TiO2 thin films deposited by

spray pyrolysis technique for photocatalytic application", *Materials Research Express*, 8(2), 2021.

[33] E. S. Gadelmawla, M. M. Koura, T. M. A. Maksoud, I. M. Elewa, and H. H. Soliman, "Roughness parameters", *Journal of Materials Processing Technology*, 123 (1), 133-145, 2002.

[34] Z. Sun, V. F. Pichugin, K. E. Evdokimov, M. E. Konishchev, M. S. Syrtanov, V. N. Kudiiarov, K. Li and S. I. Tverdokhlebov, "Effect of nitrogen-doping and post annealing on wettability and band gap energy of TiO2 thin film", *Applied Surface Science*, 500, 144048, 2020.

[35] M. Sreemany and S. Sen, "Influence of calcination ambient and film thickness on the optical and structural properties of sol-gel TiO2 thin films", *Materials Research Bulletin*, 42(1), 177-189, 2007.

[36] D.Y . Lee, J.T. Kim, J. H. Park, Y. H. Kim, I. K. Lee, M. H. Lee, and B. Y. Kim, "Effect of Er doping on optical band gap energy of TiO2 thin films prepared by spin coating", *Current Applied Physics*, 13(7),1301-1305, 2013.

[37] T.S. Senthil and M. Kang, "Transparent thin film dye sensitized solar cells prepared by sol-gel method", *Bulletin of the Korean Chemical Society*, 34(4), 1188-1194, 2013.

[38] A. Nakaruk, C. Y. Lin, D. S. Perera and C. C. Sorrell, "Effect of annealing temperature on titania thin films prepared by spin coating", *Journal of Sol-Gel Science and Technology*, 55, 328–334, 2010.

[39] T. M. Wang, S. K. Zheng, W. C. Hao and C. Wang, "Studies on photocatalytic activity and transmittance spectra of TiO2 thin films prepared by r.f. magnetron sputtering method", *Surface and Coatings Technology*, 155, (2-3),141–145, 2002.

[40] M. Sreemany and S. Sen, "A simple spectrophotometric method for determination of the optical constants and band gap energy of multiple layer TiO2 thin films", *Materials Chemistry and Physics*, 83,169-177, 2004.

[41] P. Hervé, L. K. J. Vandamme, "General relation between refractive index and energy gap in semiconductors", I*nfrared Physics & Technology*, 35 (4), 609–615, 1994.

[42] S. K. Tripathy, "Refractive indices of semiconductors from energy gaps", *Optical Materials*, 46, 240–246, 2015.

[43] A. Chanda, S. R. Joshi, V. R. Akshay, S. Varma, J. Singh, M. Vasundhara and P. Shukla, "Structural and optical properties of multilayered un-doped and cobalt doped TiO2 thin films", *Applied Surface Science*, 536, 147830 2021.

[44] S. M. Al-Shomar, "Investigation the effect of doping concentration in Ruthenium-doped TiO2 thin films for solar cells and sensors applications", *Materials Research Express*, 7, 036409, 2020.

[45] B. Houng, C. C. Liu and M. T. Hung, "Structural, electrical and optical properties of molybdenum-doped TiO2 thin films", *Ceramics International*, 39 (4), 3669–367639, 2013.

[46] M. Subramanian, S. Vijayalakshmi, S. Venkataraj and R. Jayavel, "Effect of cobalt doping on the structural and optical properties of TiO2 films prepared by sol-gel process", *Thin Solid Films*, 516, 3776–3782, 2008.

[47] C. J. Brinker, G. C. Frye, A. J. Hurd and C. S. Ashley, "Fundamentals of sol-gel dip coating", *Thin Solid Films*". 201, 97–108, 1991.

[48] P.B. Nair, V. B. Justinvictor, G. P. Daniel, K. Joy, V. Ramakrishnan, D. D. Kumar, and P. V. Thomas, "Structural, optical, photoluminescence and photocatalytic investigations on Fe doped Tio2 thin films", *Thin Solid Films*, 2014.

[49] M. M. Rahman, K. M. Krishna, T. Soga, T. Jimbo, and M. Umeno, "Optical properties and X-ray photoelectron spectroscopic study of pure and Pb-doped TiO2 thin films", *Journal of Physics and Chemistry of Solids*, 60 (2), 201-210, 1999.

[50] J. Yu, H. Yu, C. H. Ao, S. C. Lee, J. C. Yu and W. Ho, "Preparation, characterization and photocatalytic activity of in situ Fe-doped TiO2 thin films", *Thin Solid Films*, 496 (2), 273-280, 2006.

[51] F. B. Li and X. Z. Li, "Photocatalytic properties of gold/gold ion-modified titanium dioxide for wastewater treatment", *Applied Catalysis A: General*, 228 (1-2), 15-27, 2002.